Microstructure and Magnetic properties of ferrite nanoparticles synthesized by Co-precipitation method

R. Sagayaraj (sagayarajnancy@gmail.com)
St. Joseph's College of Arts and Science https://orcid.org/0000-0003-3979-6846
S.Aravazhi
Arignar Anna Arts College
G. Chandrasekaran
Pondicherry University

Research Article

Keywords: Co-precipitation, nanoparticles, ferrimagnetic properties, coercivity, Li-ion batteries, Ferrites

Posted Date: March 25th, 2021

DOI: https://doi.org/10.21203/rs.3.rs-356267/v1

Abstract

In the current research, $Cu_{0.5}Co_{0.3}Mo_{0.2}Fe_2O_4$ mixed ferrite nanoparticles have been synthesized using Co-precipitation method. XRD patterns show the development of polyphasic copper, cobalt and molybdenum mixed spinel composition. The particle size of ferrite system is 16nm and they are nanoparticles. The lattice constant was determined to be 8.368 Å used for the highest peak (311). FTIR spectroscopy shows the lower octahedral and higher tetrahedral frequency alignment of ions in the spinel ferrite leading to the octahedral 550 cm^{-1} and the tetrahedral 471 cm^{-1} vibration modes. TEM micrographs showed spherical morphology and their particle size less than 50 nm, which correlated XRD crystallite size. VSM shows excellent ferrimagnetic properties because of higher coercivity (985.29 G). These higher coercivity materials can make cathode content for Li-ion batteries.

1. Introduction

Magnetic spinel ferrites have the usual formula of 'AB_2O_4,' where 'A^{2+}' and 'B^{3+}' ions have 'tetra(A)' and 'octa [B]' voids. Oxygen ions (O^{2-}) form a cubic arrangement with iron ions placed at two separate interstices between them: tetra (A) and octa [B] voids [1, 2]. Ferrites composite have more attention because of their electrical resistance and magnetic properties when used as high-frequency devices [3]. Cubic spinel ferrites or ferrimagnetisms are a vital class of magnetic spinel material with high saturation magnetization and enormous thermal properties [4]. Unit cell of the magnetic spinel ferrite lattice contains 32 octahedral voids and 64 tetrahedral voids accessible for the respective cations, among which only 24 octahedral voids and 8 tetrahedral voids are engaged by the relevant cations [5]. Cobalt ferrite interests to us among the various magnetic spinel ferrimagnetisms and has an inverse spinel structure, where Co^{2+} cations are octahedral and Fe^{3+} cations are similarly distributed due to ionic radii in tetrahedral and octahedral voids [6]. Among spinel ferrites, cobalt spinel ferrite is significant from a biomedical point of view due to its high saturation magnetization, high permeability and no preferred magnetization path [7]. Magnetic materials (MMs) in a cluster of nano-scale materials Owing to their superior surface properties, multi-modal dimensionalities have been highly used in bio-application assortment; Improved colloidal and chemical durability, controllability, super-paramagnetic movement , low toxicity, easy preparation [8,9,10]. Magnetic nanoscale particles used in ferrofluids (magnetic nanofluids) are usually prepared in varying sizes and morphologies from ferromagnetic materials (metal materials) such as Fe, Co, Ni and ferrimagnetic materials (oxide materials) [11]. Nano materials have superior structural, electronic, electrical, magnetic properties relative to bulk materials [12]. Ferrite is typically useful in microwave gadget applications [13]. Hyperthermia is a therapeutic procedure that directly destroys tumour cells over normal cells by warming the tumour at temperatures of 41°C–45°C and combines full-body hyperthermia and selective hyperthermia [14]. Spinel nanoferrites have photocatalytic properties that are useful for different oxidation of organic compounds in wastewater and strong interest for biomedical applications [15, 16]. Due to the strong interface between nucleic acids and carboxyl groups, the surface functionalized magnetic nanoparticles facilitate the rapid and possible adsorption of viral RNAs. Due to the strong interface between nucleic acids as well as carboxyl groups,

surface-functional magnetic nanoparticles allow rapid and adsorption of viral RNAs [17]. Magnetic hyperthermia is a major mediated heat treatment that is evolving increasingly in cancer therapy. It is a medical treatment that relies on locally heated (24 degree Celsius) tissue to kill approximately 30 minutes of infected tissues, especially malignant tumors. Magnetic nanoparticle hyperthermia is desirable because it provides a means to ensure that only the expected target tissue is heated [18]. Molybdenum (Mo) Nano powder performs admirably in the production of lubricants that must withstand high temperatures. Molybdenum (Mo) based ferrite has been used as anticorrosive additives, sintering additives, hard alloys, vacuum valves, and cutting equipment for the past five decades. Mo isn't affected by oxidation. As a result, ferrite stabilizer was used, as well as the best element in steel carbon settlement [19]. Because of their low solvency and anion selectivity barrier, molybdenum ferrites are generally resistant to corrosion in sour environments [20]. When copper and molybdenum are combined, magnetic properties ranging from paramagnetic to ferromagnetic are produced. Their exposure to a magnetic field from the outside is enormous and promising. Magnetic fields attract them, and they can retain their magnetic properties even when the external field is removed [21]. Such a ferrite materials used in magnetic sensors, transformer cores, biomedical sensors, solar energy conversion, energy storage media, antenna rods, recording heads, microwave systems, magnetic cooling, ferrofluids, drug delivery, cellular therapy, tissue repair, gas detectors , hyperthermia treatment, Nano-oil, oxygen-content-control, magnetic relaxation, strain energy can be used with spinel ferrite [22- 30, 32, 34]. Many attempts have been made possible by mixing (Mo) the end member ferrites namely $CoFe_{2-x}Mo_xO_4$ [21], $ZnFe_{2-x}Mo_xO_4$ [33], $MoFe_2O_4$ [26], Fe-C_xMn-0.4Mo[35],$Co_{0.65}Zn_{0.35}Fe_{2-x}Mo_xO_4$[24], $Co_{0.5}Zn_{0.25}M_{0.25}Fe_2O_4$ (M = Ni, Cu, Mn, Mg) [36], $MnFe_{2-x}Mo_xO_4$ [37], $CuFe_{2-2x}Mo_xO_4$[38], $MnFe_{2-x}Mo_xO_4$[39], $MgFe_{2-2x}Mo_xO_4$[40], $Li_{0.3}Zn_{0.4}Mo_xFe_{2.3-x}O_4$ [41]. From TGA, the original weight loss resulted due to the removal of perennial gasses and the moisture entranced by the air environment in the spinel ferrites. This amount of reduction and saturation of weight loss shows the formation of the spinal process with the oxidation of secondary phases. The temperature with which the spinel process is formed is generally referred to as the ferritzation temperature. The occurrence of this exothermic peak clearly promotes the discharge of energy in a broad manner which is consequently used for the start of combustion and the creation of spinel phases that were in close alignment with the TG curves [10, 42]. As in TGA curve, a drop in weight is detected at 320 ^oC due to water depletion and a steady mechanism of crystallization arising from 470 ^oC to 800 ^oC nickel ferrite samples. The the meximum weight loss in the temperature range from 470 ^oC to 800 ^oC confirms the formation of a crystalline and spinal structure. The much more rapid weight loss at 320-460 ^oC is due to the elimination of water, degradation and nitrates and the deterioration of the initial mixtures [1]. From the BET review, the number of pores seen in spinel magnetic materials depends on the calculation of nitrogen gas adsorbed by the solid pores. Prepared ferrite has been found to absorb the most intense measure of nitrogen gas with a proportional weight of 0.1 to 0.9[43]. Knowledge on the precise surface area, the meso/macroscopic morphology and the existence of nano-scale gaps is critical in deciding the surface properties of nano-scale materials. For this reason, the 'Brunauer-Emmett-Teller' approach widely known as BET is very beneficial [15, 44]. In this work, we aim to extend our previous work related to Tuning of ferrites ($Co_xFe_{3-x}O_4$) nanoparticles by co-precipitation technique (SN Appl. Sci. 1(3) (2019)271) and

Structural, morphological and magnetic characters of PVP coated $ZnFe_2O_4$ nanoparticles, J Mater Sci: Mater Electron, 29(3) (2017) 2151–158. So as to realize their structural properties as a function of both magnetic specifications and Nano range particle size, especially for the correlation with microstructure (XRD) in composite to the nanoscale structure (TEM). For Mo and Cu incorporated with $CoFe_2O_4$ as improved Structural properties and magnetic properties of system for the related communities. In depth, the influence of molybdenum (Mo) strongly affected crystal structure, surface morphology, and magnetic properties of CCM-ferrite have been studied and compared to the literature view.

2. Experimental Part

2.1 Materials

Copper (II) sulfatepenthydrate ($CuSO_4.5H_2O$ assay: 98%), Cobalt (II) sulfate heptahydrate ($CoSO_4.7H_2O$), Molybdenum (VI) oxide (MoO_3 assay: 99.5%), Ferric sulfate monohydrate ($Fe_2 (SO_4)_3.H_2O$, assay: 99%), Ethanol (C_2H_5OH), Ammonia (NH_3), Polyvinylpyrrolidone (PVP) $(C_6H_9NO)_n$, assay: 98%) were purchased from Sigma Aldrich.

2.2. Characterization

The following methods have been employed in the present study to classify the as-prepared Nanomaterials. For the characterizations given below, the various instruments have specific techniques used. XRD is a good spectroscopic technique (SHIMADZU-XRD 6000) to distinguish crystalline phases, orientation, structural properties, and atomic arrangement of ferrite nanoparticles. In order to identify functional groups in nanomaterials, especially functionalized nanocatalysts (Perkin-Elmer Spectrum RXI), FT-IR is an effective spectroscopic technique. HR-TEM is a more sophisticated technique that enables a single nanoparticle (< 1 nm) to be observed and its structural morphology determined (HR-TEM: JEM-2100). To determine the percentage of elements or components in nanomaterials, EDS is a key spectroscopic technique, especially in functionalized nanocatalysts (EDS: JEM-2100).VSM is an important spectroscopic technique for the determination of ferrite nanoparticles' magnetic properties (Lakeshore VSM 7410) [45].

2.2 Synthesis of PVP coated $Cu_{0.5}Co_{0.3}Mo_{0.2}$ Fe_2O_4 (CCMF) nanoparticles

CCMF nanoparticles were employed by co-precipitation method. Temperature, pH, concentration, reaction time are potential importance to employed CCMF. The potential parameter plays an important role in the production of CCMF powders with the desired shape and size. Fig.1. explain the basic root to synthesis of CCMF ferrite nanoparticle. Copper (II) sulfate pentahydrate, Cobalt (II) sulfate heptahydrate, Molybdenum oxide, Ferric sulfate monohydrate are precursors of CCMF. They mixed by means of stoichiometric ratio (1:2). A beaker composed 75 ml distilled water with precursors. Then, PVP (1g) mixed 15ml of ionized water and used a 250 ml conical flask. It was added to the primary signature. Then 10 ml of ammonia was liquefied in 10 ml of purified water. After that, it can slowly add to the primary solution

and maintain the pH level at 11. The solution observed black. This pH value helps to change the positive surface of materials, and absorption is negatively charged with ions. As a result, it is a greater attraction for complex positive cations like Fe^{3+}/Fe^{2+}, Cu^{2+}, Co^{2+}, Mo^{3+}, Mo^{4+}, Mo^{5+} and Mo^{6+}. So, the adsorption increases at higher pH [22]. This helps to migrate cations between tetrahedral and octahedral voids for ionic radius. And it stirred the mixed solution for 4hours at 70^{o}C using a magnetic stirrer. Then ethanol and ionized water are used to remove the excess impurities present in the materials by centrifuge. For washed precipitate materials, keep the hot air oven at 100^{o}C for 4hours. Finally, they reserved a muffle furnace and annealed at 600^{o}C for 4 hours and got polycrystalline nanoparticles. Co-precipitation and ferritzation step followed such as [46, 47]:

Co-precipitation step:
$0.5Cu^{2+} + 0.3Co^{2+} + 0.2Mo^{3+} + 2Fe^{3+} + 8OH^{-} \rightarrow 0.5Cu(OH)_2 \cdot 0.3Co(OH)_2 \cdot 0.2Mo(OH)_3 \cdot 2Fe(OH)_3$
Ferritzation step:
$0.5Cu(OH)_2 \cdot 0.3Co(OH)_2 \cdot 0.2Mo(OH)_3 \cdot 2Fe(OH)_3 \rightarrow Cu_{0.5}Co_{0.3}Mo_{0.2}Fe_2O_4 + 4H_2O$

3. Results And Discussion

3.1 XRD Study

XRD patterns of CCMF represent in Fig.2. These pattern indicate that the complex nature. These structural peaks are indexed such as (220), (311), (111), (422) etc are evidence polycrystalline phase and it has magnetic ordered spinel structure. For peak reflections such as (2 2 0); (4 0 0); (3 1 1); (2 2 2); (5 1 1); (4 2 2); (4 4 0) and (5 3 3) with FCC-structure but also for the existence of impurity peaks confirming the polycrystalline phase of the present samples [42]. The lattice constant, X-ray density, dislocation density, strain and crystallite size values determined by using (311) prominent peak. These parameters are calculated by following equations [48, 49],

Crystallite size	$D = 0.9\ \lambda / \beta \cos\theta$	[nm]	(1)
Lattice constant	$a = [d^2 (h^2+K^2+l^2)]^{½}$	[Å]	(2)
X-ray density	$D_x = 8M/Na^3$	[g/cm^3]	(3)
Volume	$V = a^3$	[Å]^3	(4)
Strain	$\varepsilon = (\beta \cos\theta)/4$	[no unit]	(5)

The lattice constant (a) calculated by most intense peak (311) for CCMF is 8.368 Å due to incorporation of bigger ionic radius Mo^{3+} (0.69 Å) cations instead of comparatively small Fe^{3+} (0.64 Å) cations, which is in accordance with that stated in the literature [23,50]. By knowledge, Mo exist more chemical valance

states such as Mo^{3+}, Mo^{4+}, $Mo^{5+}$and Mo^{6+}. Mo cations did not directly replace by Fe^{2+}/Fe^{3+} actions. Hence, polycrystalline phase structure distorted or arose secondary phase in the materials (Fig.2). The First major effect of peaks in CCMF due to shifting of lower angel peaks on either side of prominent peak i.e. (311) with incorporation of Mo ions observed in the literature [44]. The second idea, when lattice constant increased due to migration of the larger ionic radius of Mo ions between two voids. However, note that there are differences in the ionic radius when that of Fe^{3+} is compared with either Mo^{3+} or Mo^{6+}. The ionic radius of Fe^{3+} (0.64 Å) is smaller than that of Mo^{3+} (0.69 Å) and larger than that of Mo^{6+} (0.59 Å). Therefore, the lattice constant CCMF indicates the function of Mo ions incorporated ferrite. It exist lower valence state than Mo^{6+} state then only lattice increase can occur. Thus, the present data clearly indicate that the Mo exists in lower chemical valance state(s) while replacing/substituting for Fe^{3+} in the CCMF lattice. The observed lattice constant (8.368 Å) is attributed to difference in ionic radii such as Fe^{3+} (0.64 Å), Mo^{3+} (0.69 Å) Mo^{6+} (0.59 Å) [51, 52]. The crystallite size of CCMF is 16 nm. Therefore, if the crystallite size (16nm) is expected to decrease, the crystal axis ratio will increase as well. Molybdenum incorporated $ZnFe_2O_4$ employed by Zein K. Heiba and repotted crystallite size, strain, X-ray density, volume is (8.1-11.9) nm, (22-41), (5.59-5.773) respectively [33]. For complex valance state cations (Mo^{3+}/ Mo^{6+}) can raise a compression stress resulting in a lattice micro strain (CCMF=0.23009) preventing the grains from growing. It is therefore confirmed that in the materials, lattice strain is generated. A micro-strain (lattice strain) means that the distance between the respective crystal planes, which is not the same, probably because of the presence of defects and stress (magnetic properties). For expect the reduction of the crystallite size with Mo content to be associated with an increase of the micro-strain for the surface-induced stress effects. So, the crystallite size of CCMF is grater then Molybdenum doped $ZnFe_2O_4$. The density and atomic weight of Mo^{3+} are 10.28 g/cm^3 and 95.94, which are greater than those of Fe^{3+} 7.874 g/cm^3 and 55.845. Thus, the overall density increase of CCMF compounds can attribute to the fact that the density and atomic weight of Mo are higher than those of Fe for which the Mo ions are substituting or replacing in CCMF [21]. Furthermore, the crystallite sizes are in good agreement with the TEM analysis results of the CCMF. The volume of unit cell is 583.857$Å^3$. It was observed that Fe^{2+} ions can be introduced into the cations Mo to give up the neutrality of charge in the ferrite materials.

3.2 FTIR study

The FT-IR spectra of CCMF showed in Fig.3, in which observe four characterizing peak between 400-4000 cm^{-1}. There are two most intense peaks observed in spectra such as 471cm^{-1} and 550cm^{-1}, which are corresponding to the tetrahedral and octahedral vibrational modes [38,39] respectively. Non magnetic metal like molybdenum (Mo) incorporated spinel ferrite; it shifts bands to the higher wave number. Hence peaks amplitude/intensity decreases for the lattice parameters modifications or crystal defects. The characteristic molybdenum (O-Mo-O) bands appear in the range 984 cm^{-1}[38, 53, 54]. The shift in the bands positions can attribute to the reduction in lattice parameters for Mo doping [39]. Lattice parameter's value depends of difference in ionic radii of Fe^{3+} and Mo^{5+} ions. Tetrahedral ionic radius of

Mo5+ ions (0.46 Å) is smaller than the tetrahedral ionic radius of Fe^{3+} ions (0.49 Å) while the octahedral ionic radius of Mo^{5+} ions (0.61 Å) is larger than the octahedral ionic radius of Fe^{3+} ions (0.55 Å)[39]. The peak at 1079 cm^{-1} refers to C–H bending mode [53]. The peak at 1632 cm^{-1} assigned to C=O band stretching [39]. 2359-3363 cm^{-1} referring to the stretching vibration of O-H bands of water molecules [39, 55].

3.3 TEM & EDX study

Fig.4 shows the TEM microstructures of CCMF and more or less spherical aggregates with the size up to 50 nm. Since the relatively large thickness of the aggregates makes it difficult to observe the bulk particles, typical features on the edges of the aggregates can still be observed. There is obviously a different contrast to the matrix in certain individual crystallites, which suggests that they are made up of heavier elements than the rest of the matrix. The micrograph shows that two forms of nanoparticles are present. Dark contrast particles showed a spherical form with a random orientation and an average size of >50 nm, consisting in a CCMF ferrimagnetic phase in the structure [36]. For the CCMF sample a closer investigation into the HR-TEM image shows the presence of two types of crystallites that can be well correlated to the XRD observations. The high value of lattice micro-strain of the materials can be best explained on the basis of charge carrier hopping between $Fe^{2+} \leftrightarrow Fe^{3+}$, $Co^{2+} \leftrightarrow Co^{3+}$, $Cu^{2+} \leftrightarrow Cu^{3+}$ and $Mo^{2+} \leftrightarrow Mo^{3+}$ ions, so that the electric dipoles align themselves along the applied alternating field [24]. Fig. 4, the adequate content of both Mo and Co additives will obviously increase the grain size of the CCMF ferrites and do not shape clearly closed pores [55]. As shown in Fig.5, The presence of all the compounds i.e., Cu, Co, Mo, Fe, O and C confirmed the formation of nanocomposite $Cu_{0.5}Co_{0.3}Mo_{0.2}Fe_2O_4$ (CCMF) and without any impurities, The Co, Mo, Cu and O signals are clearly defined, indicating the active processing of copper, cobalt, molybdenum and iron containing metal oxides. The Cu peak strength for the samples prepared using higher Cu precursor ratios has been increased.

3.4 VSM study

The magnetic properties modifications of CCMF depends crystallite size, cations orientations surface morphology and super-exchange interactions via the mediating oxygen O^{2-} anions [39]. The magnetization curves showed in Fig.6, which explained ferrimagnetic behavior. For, Coercivity (Hc) of CCMF is 985.29 G. The higher coercivity value suggests that CCMF exhibit excellent soft ferrimagnetic properties [56]. This ferrimagnetic moment (μ_B =8.808E-3) exhibits for electron spin signature. Hence, the magnetization strongly affected by cation settlement between tetrahedral sites/voids (A) and octahedral sites/voids (B). According to Neel's collinear model, three types of super exchange interactions involved such as A–B, A–A, and B–B. Here, A–B interaction is stronger than A–A and B–B interactions [41]. The saturation magnetization of CCMF is 0.20137emu/g. This lower magnetization exhibits by the substitution of Fe^{3+} by nonmagnetic Mo^{3+} ions at the B sites for ionic radius. As results migrations of Fe^{3+} in the B sites. It eliminates exchange (B-B) and super exchange (A-B) interactions [26, 57]. Similarly, same result was got for Mo doped ferrite nanoparticles [37, 40, 41]. For the present method, the

exceptionally low magnetization values derive from two sources. Primary, the ferrimagnetic activity at the B site ($Fe^{3+}\leftrightarrow Mo^{6+}$) and secondary, the small size with the local and surface canting effects associated with it [39]. Saturation magnetization of the Mo doped ferrimagnetic signature suggested that it was attributable to the net magnetic moment of ions of opposite rotations in interstitial positions. The lower remnant magnetization (Mr =0.10608 emu/g) obtained by CCMF, which can be described by substituting fewer magnetic Mo^{6+} ions on the basis of magnetic dilution. Because of, density of Fe-ions is decreased at the tetrahedral site (A) when the Fe^{3+} ions (magnetic) are replaced by Mo^{6+} ions (nonmagnetic), resulting in a small value magnetic moment and remnant magnetization from review of ligature [56]. The remnant ratio of CCMF is 0.5267. If the residual ratio is greater than 0.5, compounds have a single magnetic domain instead of a multi-magnetic domain where the residual ratio is less than 0.5 [56]. Above said concept and summarized data widely agreed that the polycrystalline ferrites with FCC phase are greatly influenced by different intrinsic and extrinsic factors such as saturation magnetization (Ms), grain size, purity, shape of particle and particle distribution [41, 58]. By modified CCMF structure materials can improved Structural and magnetic properties of system. So, it has higher coercivity (985.29G) and can be used for cathode content Li-ion batteries [23].

4. Conclusion

In depth, the influence of molybdenum (Mo) strongly affected crystal structure, surface morphology, and magnetic properties of CCM-ferrite have been studied and compared to the literature view. XRD patterns showed polyphasic copper, cobalt and molybdenum mixed ferrite spinel structure. The particle size (16 nm) and lattice constant (8.368 Å) calculated for the highest peak (311). FTIR analyzed the functional groups of the synthesized materials, which confirmed mixed spinel structure. TEM images showed spherical morphology of the nanoferrite system, where particle size from 2 to 50 nm and its good agreement with XRD. EDX spectrum ensures the purity of the nanoferrite system which showed in the sample of $Cu_{0.5}Co_{0.3}Mo_{0.2}Fe_2O_4$. The VSM reveal ferrimagnetic magnetic properties and have higher coercivity (985.29G). These synthesized ferrimagnetic material very attractive candidate for cathode content Li-ion batteries.

Declarations

Acknowledgments

Special thanks go to Nanotechnology and Crystal Growth Lab, PG and Research Department of Physics, St. Joseph's College of Arts and Science (Autonomous), Cuddalore, Tamil Nadu, India for offering wet lab facilities. One of the writers is Dr.R. Sagayaraj, thank Rev. Fr. G. Peter Rajendiram, Secretary, St. Joseph's College of Arts & Science, Cuddalore, India, for their continuing support. And I would also like to thank Rev. Fr. Dr. S. Xavier, PG and Research Department of Physics, St. Joseph's College of Arts & Science, Cuddalore, India, for their continuous assistance.

Declaration conflict of interest

No conflict of interest is there.

References

1. A.R.Chavan, S.B.Somvanshi, P.P.Khirade, K.M. Jadhav, Influence of trivalent Cr ion substitution on the physicochemical, optical, electrical, and dielectric properties of sprayed $NiFe_2O_4$ spinel-magnetic thin films. RSC Advances, 10(2020), 25143–25154
2. P.B.Kharat, S.B.Somvanshi, J.S. Kounsalye, S.S. Deshmukh, P.P. Khirade, K.M. Jadhav, Temperature dependent viscosity of cobalt ferrite / ethylene glycol ferrofluids, AIP Conf. Proc 1942 (2018), 050044
3. H.J.Kardile, S.B. Somvanshi, A.R. Chavan, A.A. Pandit, K.M. Jadhav, Effect of Cd^{2+} Doping on Structural, Morphological, Optical, Magnetic and Wettability Properties of Nickel Ferrite Thin Films, Optik (2020) 164462.
4. P.B.Kharat, S.D.More, S.B. Somvanshi, K.M. Jadhav, Exploration of thermoacoustics behavior of water based nickel ferrite nanofluids by ultrasonic velocity method, J. Mater. Sci.: Mater. Electron 30 (2019) 6564-6574
5. S.R.Patade, D.D. Andhare, S.B. Somvanshi, P.B. Kharat, S.D. More, K.M.Jadhav, Preparation and Characterizations of Magnetic Nanofluid of Zinc Ferrite for Hyperthermia Application, Nanomaterials and Energy 9 (2020) 8-13
6. S.B.Kale, S.B. Somvanshi, M.N. Sarnaik, S.D.More, S.J. Shukla, K.M. Jadhav, Enhancement in surface area and magnetization of $CoFe_2O_4$ nanoparticles for targeted drug delivery application, AIP Conf. Proc 1953 (2018) 030193
7. Thomas Dippong, Erika Andrea Levei , Iosif Grigore Deac, Emilia Neag and Oana Cadar**,** Influence of Cu^{2+}, Ni^{2+}, and Zn^{2+} Ions Doping on the Structure, Morphology, and Magnetic Properties of Co-Ferrite Embedded in SiO2 Matrix Obtained by an Innovative Sol-Gel Route, Nanomaterials 2020, 10, 580
8. S.B.Somvanshi, P.B.Kharat, M.V.Khedkar, & K.M.Jadhav, Hydrophobic to hydrophilic surface transformation of nano-scale zinc ferrite via oleic acid coating: Magnetic hyperthermia study towards biomedical applications. Ceramics, Ceram. Int. 46 (6) (2019) 7642-7653
9. S.B.Somvanshi ,S.R.Patade, D.D.Andhare, S.A.Jadhav, M.V.Khedkar, P.B.Kharat, … K.M.Jadhav, Hyperthermic evaluation of oleic acid coated nano-spinel magnesium ferrite: Enhancement via hydrophobic-to-hydrophilic surface transformation, J. Alloys Compd. 835(2020) 155422
10. S.R.Patade, D.D. Andhare, S.B. Somvanshi, S.A. Jadhav, M.V. Khedkar, & K.M. Jadhav, Self-heating evaluation of superparamagnetic $MnFe_2O_4$ nanoparticles for magnetic fluid hyperthermia application towards cancer treatment, Ceram. Int. 46 (2020), 25576-25583.
11. Prashant B. Kharat, Sandeep B. Somvanshi, Pankaj P. Khirade K. M. Jadhav, Effect of Magnetic Field on Thermal Conductivity of the Cobalt Ferrite Magnetic Nanofluids , J. Phys.: Conf. Ser. 1644 (2020) 012028

12. D D Andhare, S A Jadhav, M V Khedkar, Sandeep B. Somvanshi S. D. More and K M Jadhav, Structural and Chemical Properties of $ZnFe_2O_4$ Nanoparticles Synthesised by Chemical Co-Precipitation Technique, Journal of Physics: Conference Series 1644 (2020) 012014
13. A.Bhosale, S.B. Somvanshi, V.D. Murumkar, & K.M.Jadhav, Influential incorporation of RE metal ion (Dy^{3+}) in yttrium iron garnet (YIG) nanoparticles: Magnetic, electrical and dielectric behaviour, Ceram. Int. 46 (2020), 15372-15378.
14. Prashant B. Kharat, Sandeep B. Somvanshi, K. M. Jadhav, Multifunctional Magnetic Nano-platforms for Advanced Biomedical applications: A Brief Review, J. Phys.: Conf. Ser. 1644 (2020), 012036
15. S.A.Jadhav, S.B.Somvanshi, M.V. Khedkar, S.R. Patade, K.M. Jadhav, Magneto-structural and photocatalytic behavior of mixed Ni–Zn nano-spinel ferrites: visible light-enabled active photodegradation of rhodamine B, J. Mater. Sci.: Mater. Electron 31(2020)11352-11365
16. S.R.Patade, D.D. Andhare, S.B. Somvanshi, P.B. Kharat, K.M. Jadhav, Effect of zinc doping on water-based manganese ferrite nanofluids for magnetic hyperthermia application, AIP Conf. Proc 2265 (2020), 030557
17. S.B. Somvanshi, P. B. Kharat, T. S. Saraf, S.B. Somwanshi, S.B. Shejul, K.M. Jadhav, Multifunctional nano-magnetic particles assisted viral RNA-extraction protocol for potential detection of COVID-19, Mater. Res. Innov (2020) 1–6.
18. S.B.Somvanshi, R.V. Kumar, J.S. Kounsalye, T.S. Saraf, K.M. Jadhav, Investigations of structural, magnetic and induction heating properties of surface functionalized zinc ferrite nanoparticles for hyperthermia applications , AIP Conf. Proc 2115 (2019), 030522
19. S.S. Rathore, M.M. Salve, V.V. Dabhade, Effect of Molybdenum Addition on the Mechanical Properties of Sinter-forged Fe-Cu-C Alloys, J. Alloys Compd. 649 (2015)988-995
20. Martin Monnot, Virginie Roche, Rafael Estevez, Marc Mantel, Ricardo P.Nogueira, Molybdenum effect on the Sulfide Stress Corrosion of a super martensitic stainless steel in sour environment highlighted by Electrochemical Impedance Spectroscopy, Electrochim. Acta. 252(2017)58-66
21. Cristian Orozco, Alejandra Melendez, Sandeep Manandhar, Srinivasa Rao Rao Singamaneni, Kongara M. Reddy, Kinjal Gandha, Ikenna Nlebedim, and Chintalapalle V Ramana , Effect of Molybdenum Incorporation on the Structure and Magnetic Properties of Cobalt Ferrite, J. Phys. Chem. C 121(2017)25463–25471
22. R.Sagayaraj, S.Aravazhi, C.Selva kumar, S.Senthil kumar, & G.Chandrasekaran, Tuning of ferrites ($Co_xFe_{3-x}O_4$) nanoparticles by co-precipitation technique, SN Appl. Sci. 1(3) (2019)271
23. Z.K.Heiba, N.Y.Mostafa, & O.H.Abd-Elkader, Structural and magnetic properties correlated with cation distribution of Mo-substituted cobalt ferrite nanoparticles, J. Magn. Magn. Mater. 368 (2014)246–251
24. A.K. Pradhan, P.R. Mandal, K. Bera, S. Saha and T.K. Nath, The effect of Mo doping on the structural and dielectric properties of Co-Zn ferrite, Physica B Condens. Matter**,** 525(2017)1-6

25. T.Jia, R.Wang, & R.Xu, Performance of $MoFe_2O_4$–$NiFe_2O_4$/Fullerene-added nano-oil applied in the domestic refrigerator compressors, Int JRefrig, 45(2014) 120–127
26. T.Katayama, Y.Kurauchi, S.Mo, K.Gu, A.Chikamatsu, L.Galiullina, & T.Hasegawa, P-type Conductivity and Room-temperature Ferrimagnetism in Spinel $MoFe_2O_4$ Epitaxial Thin Film, Cryst. Growth Des 19 (2019)902–906
27. J.Ding, L.Wang, A.Roy, & J.Ghose, Magnetic relaxation in spinel Mo-ferrite and Ti substituted Mo-ferrite, Eur Phys J B 27 (2002) 49–54
28. H.Chen, Z.Yang, C.Zhang, K.Zhu, & S.van der Zwaag, On the transition between grain boundary ferrite and bainitic ferrite in Fe–C–Mo and Fe–C–Mn alloys: The bay formation explained, Acta Mater. 104(2016) 62–71
29. X.Hao, J.Dong, X.Mu, J.Wei, C.Wang, & W.Ke, Influence of Sn and Mo on Corrosion Behavior of Ferrite-pearlite Steel in the Simulated Bottom Plate Environment of Cargo Oil Tank. J Mater Sci Technol 35 (2019) 799–811.
30. B.HU, Q.CAI, & H.WU, Kinetics of Precipitation Behavior of Second Phase Particles in Ferritic Ti-Mo Microalloyed Steel, J. Iron SteelRes. Int. 20(7) (2013)69–77.
31. B.HU, Q.CAI, & H.WU, Influence of Mo on Growth and Coarsening of Nanometer-sized Carbides in Low-alloy Ferritic Steels Containing Ti, J. Iron Steel Res. Int. 21(2014) 878–885
32. Dan Song, Jun Hao, Falin Yang , Huande Chen, Ningning Liang , Yuanyuan Wu , Jianchun Zhang , Han Ma , Edwin Eyram Klu , Bo Gao , Yanxin Qiao , Jiapeng Sun, Jinyang Jiang,Corrosion behavior and mechanism of Cr–Mo alloyed steel: Role of ferrite/bainite duplex microstructure. J. Alloys Compd, 809(2019) 151787
33. Z.K.Heiba, M.B.Mohamed, & A.M.Wahba, Effect of Mo substitution on structural and magnetic properties of Zinc ferrite nanoparticles. J. Mol. Struct, 1108(2016) 347–351.
34. A.Roy, J.Ghose, A.Ray, & R.Ranganathan, Magnetic studies on Zn-substituted molybdenum ferrite, J. Magn. Magn. Mater, 202(1999) 359–364.
35. W.W.Sun, H.S.Zurob, & C.R.Hutchinson, Coupled solute drag and transformation stasis during ferrite formation in Fe-C-Mn-Mo, Acta Mater. 139(2017)62–74
36. R.-G.Ciocarlan, E.M.Seftel, M.Mertens, A.Pui, M.Mazaj, N.Novak Tusar, & P.Cool, Novel magnetic nanocomposites containing quaternary ferrites systems $Co_{0.5}Zn_{0.25}M_{0.25}Fe_2O_4$ (M = Ni, Cu, Mn, Mg) and TiO_2 -anatase phase as photocatalysts for wastewater remediation under solar light irradiation, Mater Sci Eng B 230(2018)1–7
37. F.Al-Mokdad, Z.Bitar, R.S.Hassan, N.Yaacoub, & R.Awad, Effect of molybdenum doping on the structural and magnetic properties of $MnFe_2O_4$ magnetic nanoparticles,Appl. Phys. A 126, 495 (2020)
38. G.Mitran, S.Chen, & D.-K.Seo, Molybdenum Dopped Copper Ferrites as Active Catalysts for Alcohols Oxidative Coupling. Materials 12(2019)1871

39. F.Al-Mokdad, R.S.Hassan, & R.Awad, Physical and Dielectric Properties of $MnFe_2O_4$ Doped by Mo, Current Nanomaterials 4(2019)125-136
40. N.Y.Mostafa, Z.Zaki, M.M.Hessien, A.A.Shaltout, & M.Alsawat, Enhancing saturation magnetization of Mg ferrite nanoparticles for better magnetic recoverable photocatalyst, Appl. Phys. A, 124(12) (2018).
41. Y.Gao, & Z.Wang, Effect of Mo substitution on the structural and soft magnetic properties of Li–Zn ferrites, J. Sol-Gel Sci. Technol 91(2019) 111–116.
42. S.B.Somvanshi, M.V. Khedkar, P.B. Kharat, K.M. Jadhav, Influential diamagnetic magnesium (Mg^{2+}) ion substitution in nano-spinel zinc ferrite ($ZnFe_2O_4$): Thermal, structural, spectral, optical and physisorption analysis, Ceram. Int. 46(2019) 8640-8650
43. Ravikumar M Borade et al, Spinel zinc ferrite nanoparticles: an active nanocatalyst for microwave irradiated solvent free synthesis of chalcones, Mater. Res. Express 7 (2020) 016116
44. S.B.Somvanshi, S.A. Jadhav, M.V. Khedkar, P.B. Kharat, S.D. More, K.M. Jadhav, Structural, thermal, spectral, optical and surface analysis of rare earth metal ion (Gd3+) doped mixed Zn–Mg nano-spinel ferrites , Ceram. Int. 46 (2020), 13170-13179
45. M.Kazemi, M.Ghobadi, & A.Mirzaie, Cobalt ferrite nanoparticles ($CoFe_2O_4$ MNPs) as catalyst and support: magnetically recoverable nanocatalysts in organic synthesis, Nanotechnol. Rev, 7(1) (2018)43–68
46. R.Sagayaraj, M.Jegadheeswari, S.Aravazhi, G.Chandrasekaran, & A.Dhanalakshmi, Structural, Spectroscopic and Magnetic Study of Nanocrystalline Terbium–Nickel Ferrite by Oxalate Co-Precipitation Method. Chemistry Africa 3 (2020) 955-963
47. R.Sagayaraj, T.Dhineshkumar, A.Prakash, S.Aravazhi, G.Chandrasekaran, D.Jayarajan, & S.Sebastian, Fabrication, Microstructure, Morphological and Magnetic Properties of W-type ferrite by Co-precipitation method: Antibacterial activity. Chem. Phys. Lett 759 (2020) 137944.
48. R.Sagayaraj, S.Aravazhi, G.Chandrasekaran, Effect of Zinc Content on Structural, Functional, Morphological, Resonance, Thermal and Magnetic Properties of $Co_{1-x}Zn_xFe_2O_4$/PVP Nanocomposites. J Inorg Organomet Polym Mater. 29(2019) 2252–2261.
49. R.Sagayaraj, S.Aravazhi, G.Chandrasekaran, Synthesis, Spectroscopy, and Magnetic Characterizations of PVP-Assisted Nanoscale Particle. J Supercond Nov Magn31(2018) 3379–3386
50. Ashok V. Humbe , Jitendra S. Kounsalye,Sandeep B. Somvanshi , Arun Kumar , K. M. Jadhav, Cation Distribution, Magnetic and Hyperfine Interaction Studies of Ni-Zn Spinel Ferrites: Role of Jahn Teller ion (Cu^{2+}) Substitution, Mater. Adv., 2020, 1, 880-890
51. V.A.Bharati, S.B. Somvanshi, A.V. Humbe, V.D.Murumkar, V.V. Sondur, K.M. Jadhav, Influence of trivalent Al–Cr co-substitution on the structural, morphological and Mössbauer properties of nickel ferrite nanoparticles, J. Alloys Compd. 821(2019)153501
52. A.Bhosale, S.B. Somvanshi, V.D. Murumkar, K.M.Jadhav,. Influential incorporation of RE metal ion (Dy^{3+}) in yttrium iron garnet (YIG) nanoparticles: Magnetic, electrical and dielectric behaviour, Ceram.

Int. 46(2020)15372-15378

53. P.Fakhimi, A.Bezaatpour, M.Amiri, S.Szunerits, R.Boukherroub, & H.Eskandari, Manganese Ferrite Nanoparticles Modified by Mo(VI) Complex: Highly Efficient Catalyst for Sulfides and Olefins Oxidation Under Solvent-less Condition. ChemistrySelect 4 (2019) 7116–7122
54. N.Tariq, R.Fatima, A.Rahman, S.Zulfiqar, M.F.Warsi, & I.Shakir, Synthesis and characterization of $MoO_3/CoFe_2O_4$ nanocomposite for photocatalytic applications. Ceram. Int. 46(2020) 21596-21603
55. H.Su, H.Zhang, X.Tang, & Y.Jing, Effects of MoO_3 and WO_3 additives on densification and magnetic properties of highly permeable NiCuZn ferrites. Mater. Chem. Phys, 102(2-3)(2007) 271–274.
56. M.A.Malana, R.B.Qureshi, M.N.Ashiq, & M.F.Ehsan, Synthesis, structural, magnetic and dielectric characterizations of molybdenum doped calcium strontium M-type hexaferrites, Ceram. Int. 42(2016) 2686–2692.
57. Y.Gao, Z.Wang, J.Pei, & H.Zhang, Structure and magnetic properties correlated with cation distribution of $Ni_{0.5-x}$ Mo_x $Zn_{0.5}Fe_2O_4$ ferrites prepared by sol-gel auto-combustion method, Ceram. Int. 44(2018) 20148-20153.
58. Y.Wang, H.Zhou, H.Qi, L.Ren, Z.Xu, & Z.Yue, Sintering, microstructure and magnetic properties of low temperature co-fired NiCuZn ferrites with Nb_2O_5 and MoO_3 additions. Ceram. Int. 41(2015) 12253–12257.

Figures

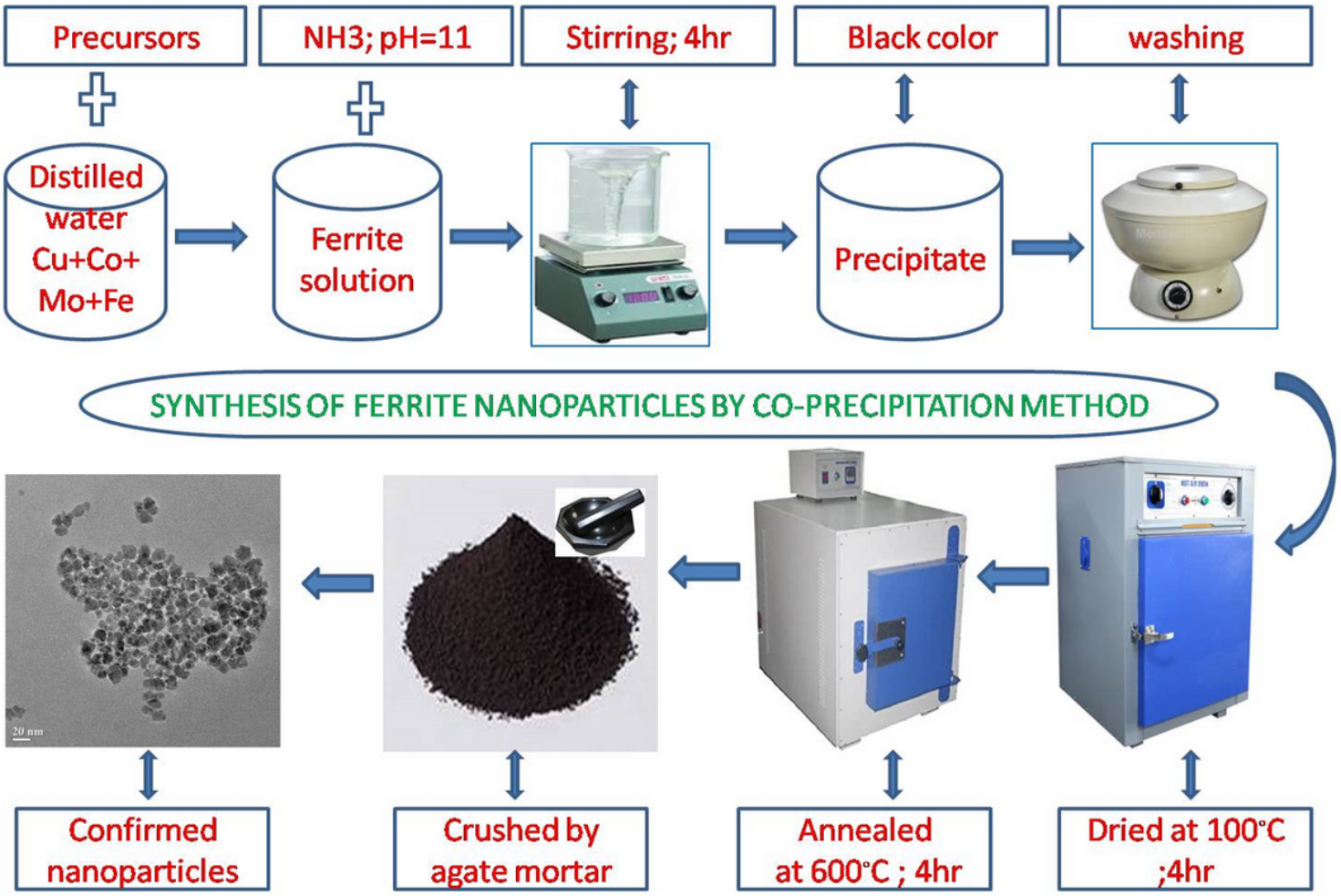

Figure 1

Synthesis of CCMF ferrite nanoparticles

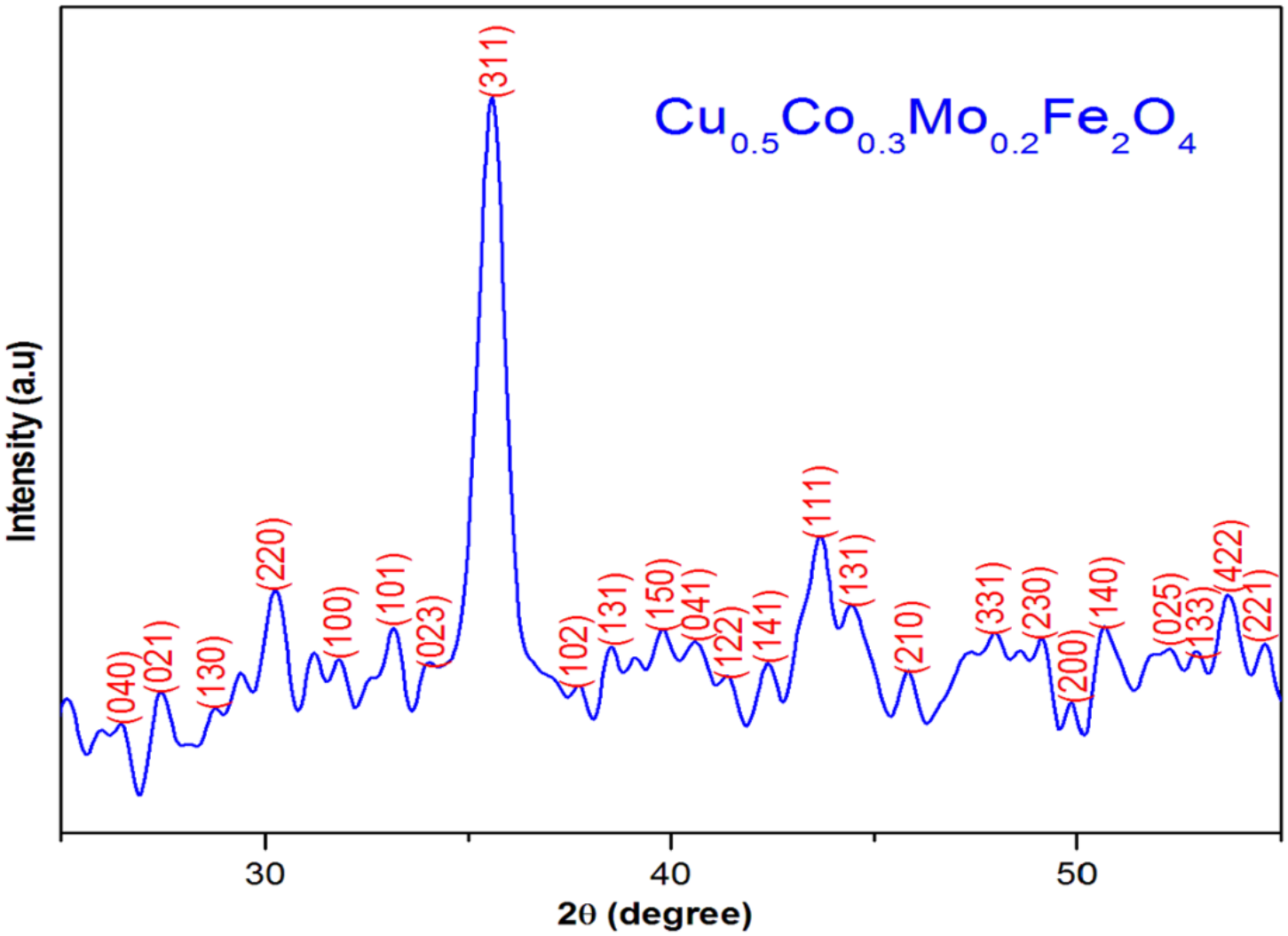

Figure 2

XRD patterns of CCMF ferrite nanoparticles

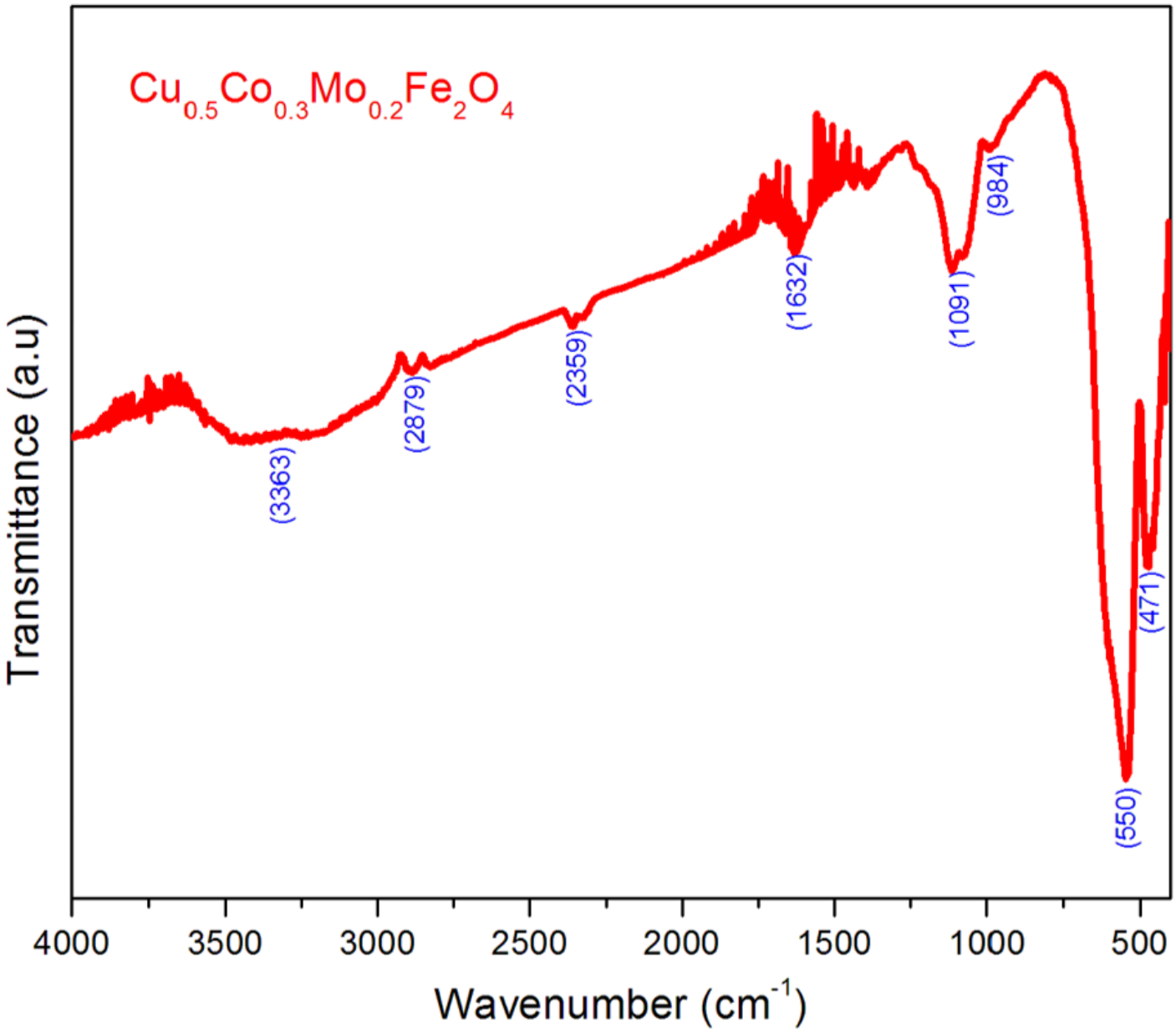

Figure 3

FTIR patterns of CCMF ferrite nanoparticles

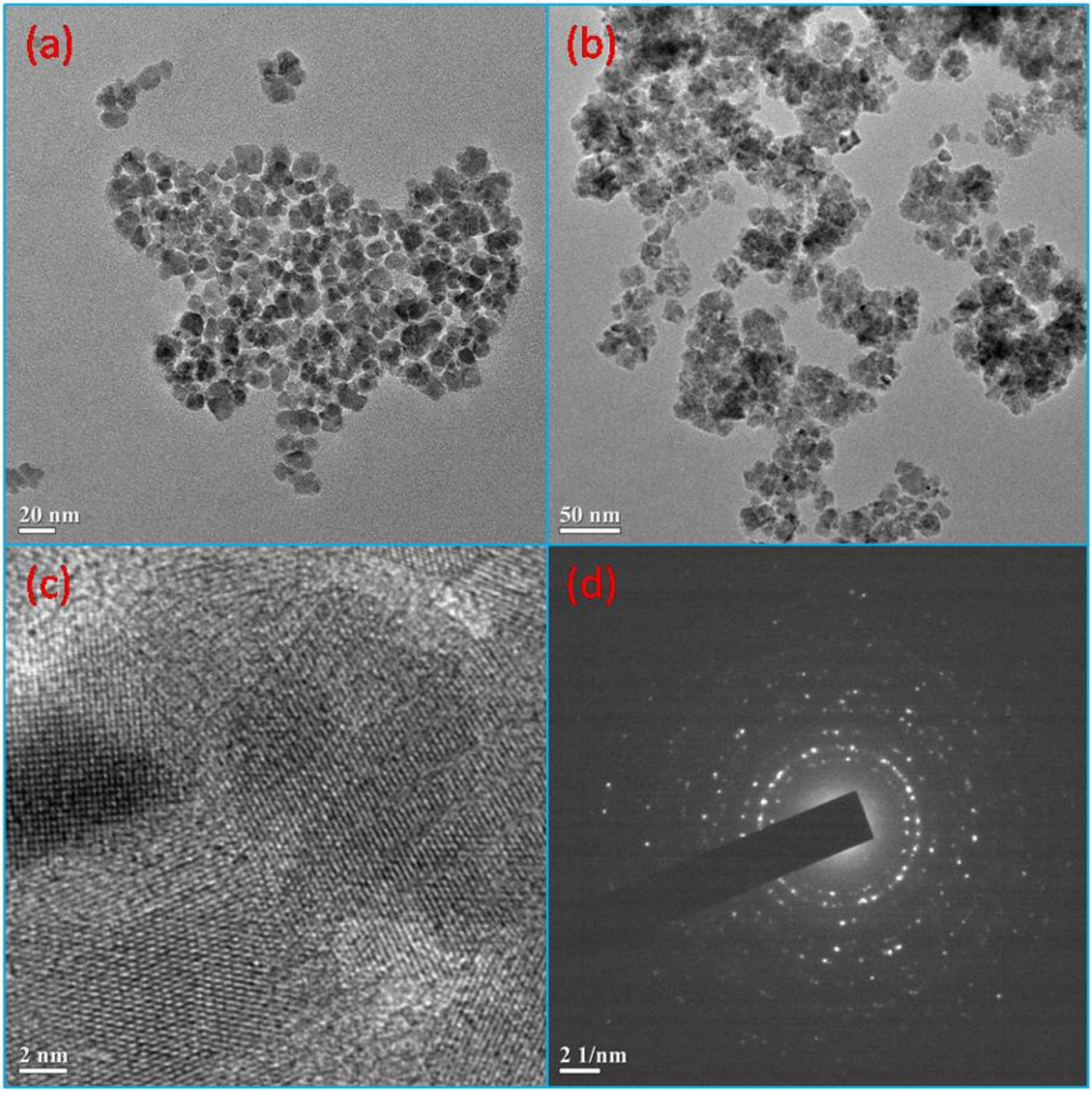

Figure 4

TEM micrographs of CCMF ferrite nanoparticles

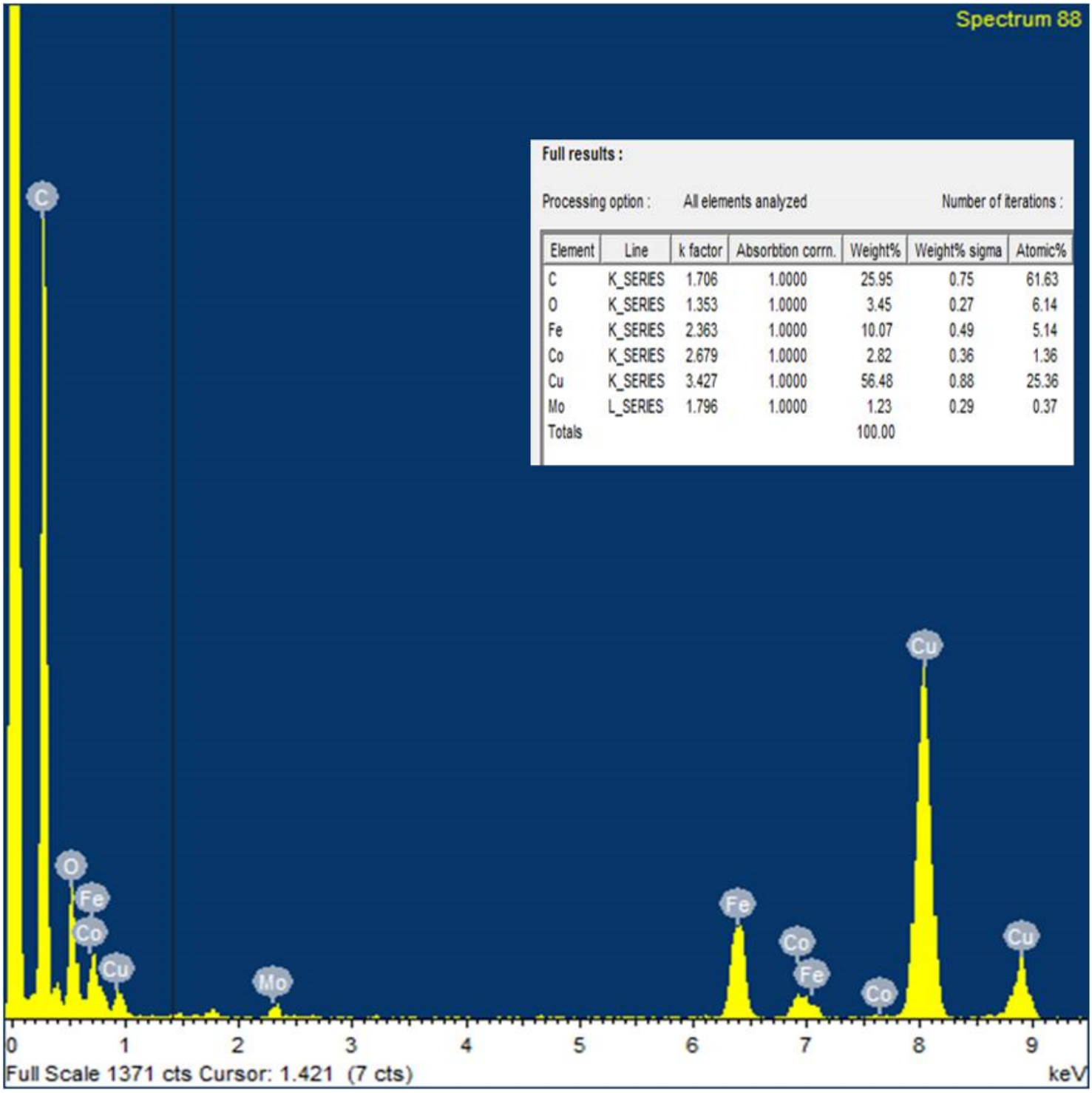

Figure 5

EDX of CCMF ferrite nanoparticles

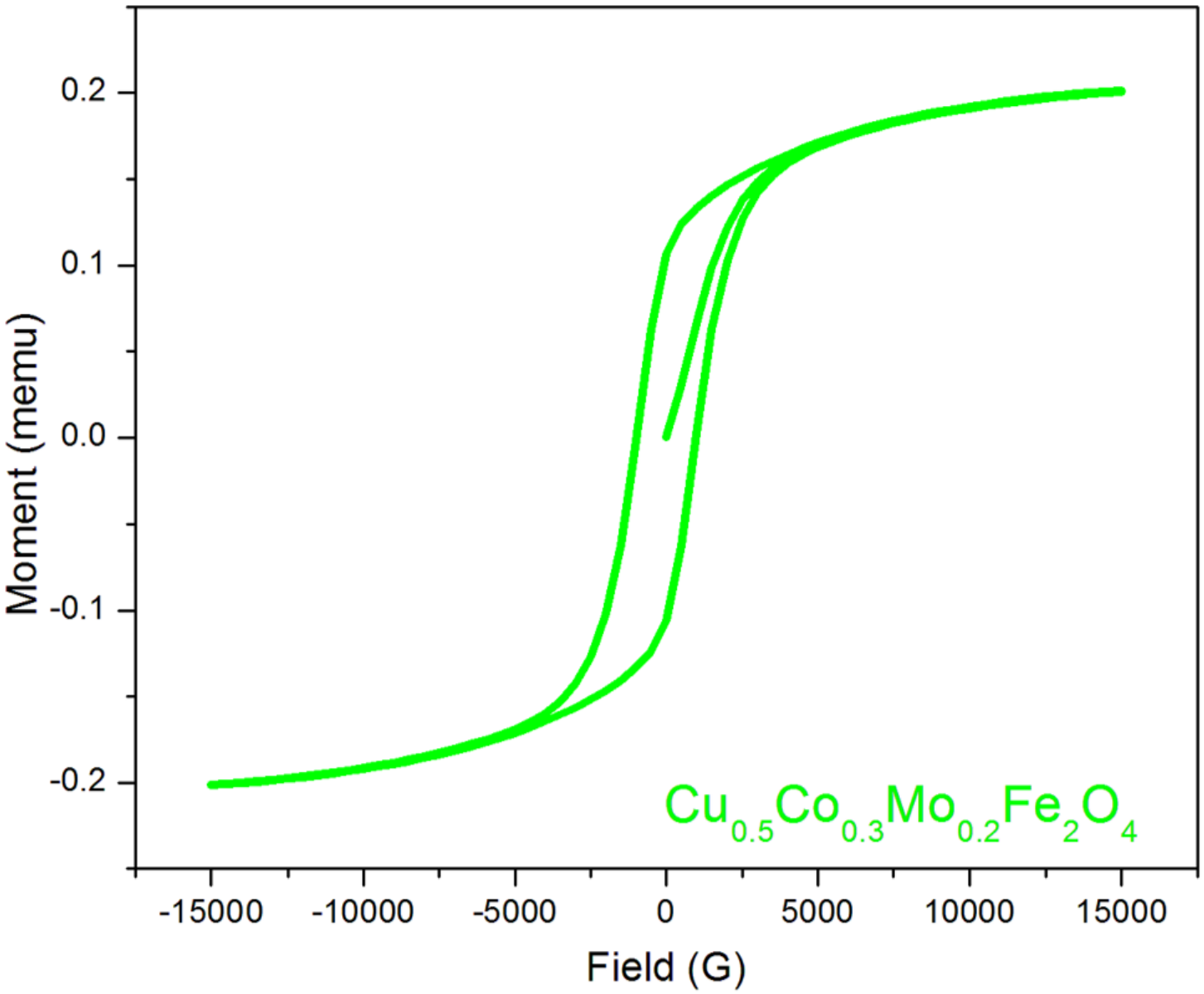

Figure 6

VSM of CCMF ferrite nanoparticles